INTERNATIONAL JOURNAL FOR NUMERICAL AND ANALYTICAL METHODS IN GEOMECHANICS
Int. J. Numer. Anal. Meth. Geomech. 2014; **38**:1431–1452
Published online 18 March 2014 in Wiley Online Library (wileyonlinelibrary.com). DOI: 10.1002/nag.2257

Microplane damage model for jointed rock masses

Xin Chen[1,2,*,†] and Zdeněk P. Bažant[2]

[1]*School of Mechanics and Civil Engineering, China University of Mining and Technology (Beijing), Beijing, 100083, China*
[2]*Department of Civil and Environmental Engineering, Northwestern University, Evanston, IL 60208, U.S.A.*

SUMMARY

The paper presents a new microplane constitutive model for the inelastic behavior of jointed rock masses that takes into account the mechanical behavior and geometric characteristics of cracks and joints. The basic idea is that the microplane modeling of rock masses under general triaxial loading, including compression, requires the isotropic rock matrix and the joints to be considered as two distinct phases coupled in parallel. A joint continuity factor is defined as a microplane damage variable to represent the stress-carrying area fraction of the joint phase. Based on the assumption of parallel coupling between the rock joint and the rock matrix, the overall mechanical behavior of the rock is characterized by microplane constitutive laws for the rock matrix and for the rock joints, along with an evolution law for the microplane joint continuity factor. The inelastic response of the rock matrix and the rock joints is controlled on the microplane level by the stress–strain boundaries. Based on the arguments enunciated in developing the new microplane model M7 for concrete, the previously used volumetric–deviatoric splits of the elastic strains and of the tensile boundary are avoided. The boundaries are tensile normal, compressive normal, and shear. The numerical simulations demonstrate satisfactory fits of published triaxial test data on sandstone and on jointed plaster mortar, including quintessential features such as the strain softening and dilatancy under low confining pressure, as well as the brittle–ductile transition under higher confining pressure, and the decrease of jointed rock strength and Young's modulus with an increasing dip angle of the joint. Copyright © 2014 John Wiley & Sons, Ltd.

Received 21 August 2013; Revised 15 December 2013; Accepted 3 January 2014

KEY WORDS: rock; microplane model; joint; constitutive model; inelastic behavior; damage mechanics; failure; geomaterials

1. INTRODUCTION

Similar to other quasibrittle materials such as concrete, intact rocks exhibit complex nonlinear inelastic behavior characterized by pressure sensitivity in triaxial tests, strain softening, dilatancy at low pressures, and brittle–ductile transition at high confinement. Unlike materials such as concrete, the behavior of rock mass is complicated by the properties and geometry of the preexisting joints. Compared with the intact rock, the rock mass is weaker, more deformable, and highly anisotropic. In the microstructure, deformation of rock mass leads to microcrack initiation, propagation and coalescence, crack opening or closing, and frictional slip on cracks or joints. These mechanisms cause strain-softening behavior, which in turn engenders size effects. The size effects, documented in South African mines already half a century ago [1], are, unfortunately, still widely ignored in the practice of geomechanics, although they are important for the safety of large scale mining excavations, tunnels and open excavations, stability of rock slopes, and prediction of rock slides. The strain softening also plays a major role in assessing the effects of explosion, impact, and ground shock.

For larger rock masses, an equivalent continuum model must inevitably be used. Because of strain softening, the theory of plasticity is inapplicable. The continuum damage mechanics, by now a classical

*Correspondence to: Xin Chen, School of Mechanics and Civil Engineering, China University of Mining and Technology (Beijing), Beijing 100083, China.
†E-mail: chx@cumtb.edu.cn

approach, has been adopted widely [2–4], although the material localization instabilities inherent to the strain-softening aspect of continuum damage mechanics have been ignored in most studies. The basic concept of continuum damage mechanics was introduced by Kachanov [5] and Rabotnov [6] for simple one-dimensional problems. A scalar damage variable, which represents the net stress-carrying cross section area fraction and gradually decreases as a result of the growth of microscopic defects (cracks and voids), was introduced to define the effective stress or true stress transmitted across the undamaged part of the cross section (the stress concentrations due to cracks and voids were ignored, for simplicity). A constitutive law for the undamaged part of the material characterizes the relationship of the effective stress to the strain. The generalization of the Kachanov–Rabotnov's damage concept for anisotropic damage has turned out to be rather difficult when the modeling was limited to the classical macroscopic tensorial approach, see, for example, Carol *et al.* [7] and Lemaitre *et al.* [8]. One advantage of the microplane model is that it makes the anisotropic generalization much easier.

The salient feature of the microplane model is that the constitutive law is written in terms of vectors rather than tensors and that these vectors act on planes of specific orientation. The advantage is that physical phenomena with distinct orientation, such as crack opening or frictional slip, can be directly reflected in the constitutive law, which facilitates its formulation. Another advantage is that the huge vertex effect observed in experiments with a nonproportional loading path in the stress space can be captured automatically [9, 10]. Since 1983, microplane models have been developed for concrete [11–15], clays [16], soils [17], rocks [18], orthotropic fiber composites, orthotropic foam, shape-memory alloy and annulus fibrosus; see [9, 12, 13] for a detailed review.

To provide better insight into the physical mechanism while adhering to the basic framework of continuum damage mechanics, microplane models based on geometric damage were proposed to separate the independent effect of geometrical characteristic [7, 19]. In these models, the concept of effective stress and the hypothesis of strain equivalence were reformulated on the microplane level, and geometric damage variables could be defined on the microplanes so as to represent a different reduction of the net stress-carrying area fraction in different directions, which is impossible in tensorial models. By adopting a set of damage variables at microplane level and assuming kinematic constraint between macrostrains and microplane strains, and static constraint between effective macro stresses and microplane effective stresses, Carol and Bažant [7] obtained a fourth-order macroscopic secant stiffness tensor for the damaged material, which is a product of the pure geometric damage tensor and the stiffness tensor of the virgin material. By defining a single damage variable on microplanes as an orientation distribution function (ODF) and an effective stress vector on the microplanes, and assuming static constraint between macro nominal stresses and microplane nominal stresses, Yang *et al.* [19] showed that the second-order effective stress tensor of Murakami [20] can be recovered as the second-order fabric tensor of the effective stress vector. Furthermore, they proved that the anisotropic yield criteria of damaged materials whose matrix follows von Mises and Drucker–Prager yield criteria possess the form of the famous Hill criterion [21] and its extension by Liu to pressure-sensitive materials [22], in which the parameters are related to the fabric tensors of the microplane damage variable.

However, the effective stress concept, characterizing the stress-carrying and stress reduction mechanisms because of cracks and joints, makes sense only for tensile loading. It is not suitable for general triaxial loading and is certainly insufficient for compressive loading. The basic idea of this paper is that, in order to take into account the stress-carrying capacity of the discontinuities under compressive load, it is more reasonable to treat the intact rock (the rock matrix), and the rock joints and cracks, as mechanically distinct phases. This idea is developed in what follows.

2. BASIC HYPOTHESES

Our objective is to construct the constitutive model for the average behavior of a representative volume element of a rock mass (Figure 1(a)), including the joints or cracks. We choose the formalism of the microplane model in which the constitutive model is defined in terms of stress and strain vectors acting on a generic plane of any orientation, called the microplane. The constitutive model is defined by the relations between the stresses and strains on the microplane. To characterize the inelastic deformations of rock with softening damage, we introduce the following three hypotheses.

DOI: 10.1002/nag

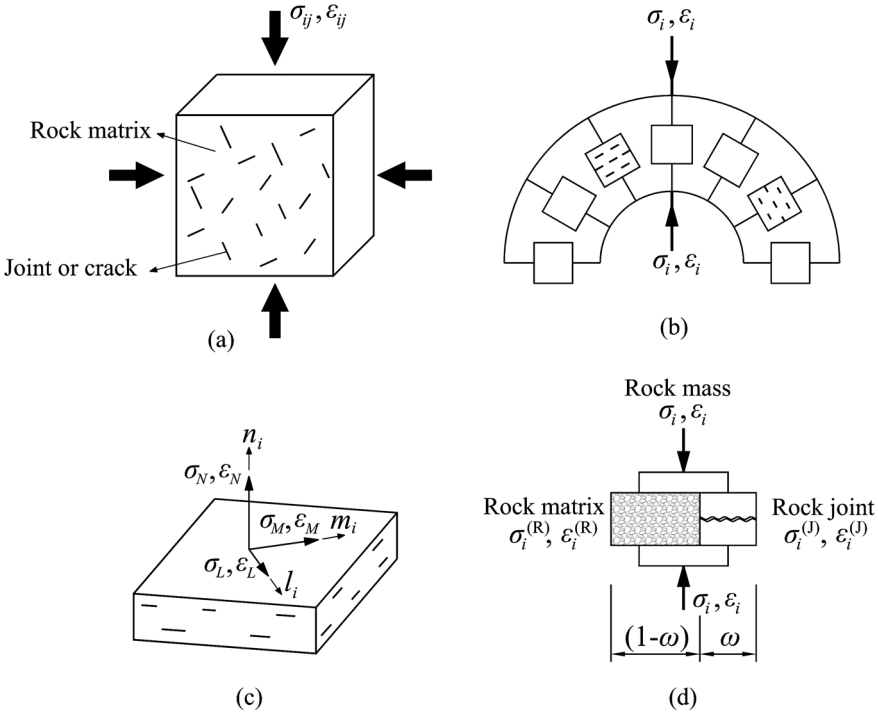

Figure 1. (a) A representative volume element of the rock mass, (b) micoplane system of the representative volume element, (c) the unit vectors on microplane, and (d) parallel coupling of the rock matrix phase and the rock joint phase on microplane.

Hypothesis I

The constitutive relations for each microplane capture the effect of only those joints or cracks whose plane is parallel to the microplane (Figure 1(b)), and the interaction among different sets of joints or cracks is considered implicitly through the correlation of microplanes with various orientations.

Hypothesis II

On each microplane, the two phases, that is, the rock matrix and the rock joint, are mechanically connected in parallel to form a combined system, the rock mass. According to the parallel coupling, the total force applied on the combined system (Figure 1(c)) is a sum of the forces acting on the two phases while the relative displacements of these phases are the same (Figure 1(d)). This hypothesis makes it possible to decompose the overall damage softening effect of the microplane system into two parts, one for the geometric part, which reflects the preexisting geological structure and the progressive cracking process, and the other for the mechanical part, which characterizes the response of the rock joints or cracks.

Hypothesis III

A kinematic constraint exists between the microplanes and the macroscopic continuum. That is, the strains on any microplane are the resolved components of the continuum (or macroscopic) strain tensor. The kinematic constraint is necessary to ensure the stability of postpeak strain softening [11] (the static constraint, in which the microplane stresses are the resolved components of the continuum stress tensor, would not ensure stability[15]).

3. MICROPLANE DAMAGE VARIABLE AND ITS FABRIC TENSORS

Rocks or rock masses commonly contain discontinuities, which are planes of weakness or surfaces of separation. They include geological features such as bedding planes, faults, shear zones, joints,

DOI: 10.1002/nag

fractures, and cracks. To characterize their effect, the concept of geometrical damage tensors, called in geomechanics the fabric tensors, is often used [4, 23, 24].

For example, Oda *et al*.[23] defined second-order and fourth-order fabric tensors for cracked rocks:

$$F_{ij} = \int_{\Omega} F(\mathbf{n}) n_i n_j \mathrm{d}\mathbf{n}, \quad F_{ijkl} = \int_{\Omega} F(\mathbf{n}) n_i n_j n_k n_l \mathrm{d}\mathbf{n}, F(\mathbf{n}) = 2\pi\rho \int_0^{\infty} r^3 f(\mathbf{n}, r) \mathrm{d}r \tag{1}$$

where, ρ, r, and $f(\mathbf{n},r)$ are volume density, radius, and probability density function of cracks. Kawamoto *et al*. [4] proposed a geometric damage tensor:

$$\Omega_{ij} = \sum_{k=1}^{N} \lambda^{(k)} n_i^{(k)} n_j^{(k)}, \quad \lambda^{(k)} = \frac{l}{V} a^{(k)} \tag{2}$$

where $a^{(k)}$ is the size of the k-th cracks in a volume V of the rock mass that consists of intrinsic cell elements with length l. Swoboda *et al*. [24] used a second-order geometric tensor to characterize the effect of parallel joints:

$$\Omega_{ij} = \omega n_i n_j \tag{3}$$

where ω is the separation factor of a set of joints of one orientation, which is taken as the crack density.

These fabric tensors contain dyadic products of the unit normal vectors of the joint planes, multiplied by an orientation dependent scalar function related to geometrical parameters, which was called by Kanatani [25] an ODF. As already pointed out by Lubarda and Krajcinovic [26], each of these fabric tensors is only a tensorial approximation of the actual ODF, which may or may not be sufficiently accurate for a given case.

In this work, a scalar-valued ODF, called joint continuity factor, $\omega = \omega(\boldsymbol{n})$, is selected as the geometrical damage variable on the microplane. It is analogous to the damage variable in damage mechanics, which is defined as the area fraction of the rock joint phase. It also characterizes the separation of the joints by the rock matrix on the microplane and may be regarded as the average measure of all the geometrical features of the joints or cracks on the microplane, such as the persistence, spacing, density, and arrangement pattern.

The value of joint continuity factor is always between 0 and 1. For a microplane with continuous joints or cracks uninterrupted by the rock matrix, $\omega(\boldsymbol{n}) = 1$; for a microplane without any joint or crack, $\omega(\boldsymbol{n}) = 0$; for a microplane containing discontinuous joints or cracks, $0 < \omega(\boldsymbol{n}) < 1$.

According to ODF analyses [25, 27], the joint continuity factor $\omega(\boldsymbol{n})$ can be approximated by fabric tensors with different accuracy:

$$\begin{aligned} &\omega(\mathbf{n}) \approx \rho_0, \\ &\omega(\mathbf{n}) \approx \rho_2 = \rho_{ij} n_i n_j, \\ &\omega(\mathbf{n}) \approx \rho_4 = \rho_{ijkl} n_i n_j n_k n_l, \ldots. \end{aligned} \tag{4}$$

Here, ρ_0, ρ_{ij}, and ρ_{ijkl} are the zero-order, second-order, and fourth-order fabric tensors of the second kind of the ODF $\omega(\boldsymbol{n})$, respectively.

Through successive contractive manipulation of the least-square minimization of their approximation differences, these fabric tensors of the second kind can be expressed in terms the fabric tensors of the first kind as follows:

$$\begin{aligned} \rho_0 &= \Omega_0, \\ \rho_{ij} &= \frac{3}{2}\left(5\Omega_{ij} - \Omega_0 \delta_{ij}\right), \\ \rho_{ijkl} &= \frac{15}{8}\left(21\Omega_{ijkl} - 14\Omega_{(jl}\delta_{ik)} + \Omega_0 I_{ijkl}\right), \ldots \end{aligned} \tag{5}$$

where $\Omega_{(ij}\delta_{kl)} = \frac{1}{6}\left(\Omega_{ij}\delta_{kl} + \Omega_{ik}\delta_{jl} + \Omega_{il}\delta_{jk} + \Omega_{jk}\delta_{il} + \Omega_{jl}\delta_{ik} + \Omega_{kl}\delta_{ij}\right)$, $I_{ijkl} = \frac{1}{3}\left(\delta_{ij}\delta_{kl} + \delta_{ik}\delta_{jl} + \delta_{il}\delta_{jk}\right)$.

DOI: 10.1002/nag

Here, the fabric tensors of the first kind Ω_0, Ω_{ij}, and Ω_{ijkl} can be calculated from the discrete directional data of joints or cracks in a volume of the rock mass:

$$\begin{aligned}\Omega_0 &= \frac{1}{2\pi}\int_{\Omega}\omega(\mathbf{n})\mathrm{d}\Omega \approx \sum_{\mu=1}^{N_m} w_\mu \omega^{(\mu)},\\ \Omega_{ij} &= \frac{1}{2\pi}\int_{\Omega}\omega(\mathbf{n}) n_i n_j \mathrm{d}\Omega \approx \sum_{\mu=1}^{N_m} w_\mu \omega^{(\mu)} n_i^{(\mu)} n_j^{(\mu)},\\ \Omega_{ijkl} &= \frac{1}{2\pi}\int_{\Omega}\omega(\mathbf{n}) n_i n_j n_k n_l \mathrm{d}\Omega \approx \sum_{\mu=1}^{N_m} w_\mu \omega^{(\mu)} n_i^{(\mu)} n_j^{(\mu)} n_k^{(\mu)} n_l^{(\mu)}, \ldots\end{aligned} \tag{6}$$

where the integral over the surface of a unit hemisphere Ω is given by $\int_{\Omega}(\cdot)\mathrm{d}\Omega = \int_0^{2\pi}\int_0^{\pi/2}(\cdot)\sin\phi \mathrm{d}\phi\mathrm{d}\theta$, ϕ and θ are the spherical angles, N_m is the number of the numerical integration points on a unit hemisphere surface, and w_μ, $n_i^{(\mu)}$, and $\omega^{(\mu)}$ are the weight, the unit normal vector, and the joint continuity factor of the μ-th microplane, respectively.

The integral for a spherical surface is approximated according to the optimal Gaussian integration formulas. For approximations with 21, 37, and 61 integration points per hemisphere, the unit vectors, and the weights were derived in Bažant and Oh [11].

4. RELATIONS BETWEEN THE MACRO-CONTINUUM AND MICROPLANE STRAINS AND STRESSES

Let σ_{ij} and $\varepsilon_{ij}, i,j=1,2,3$ be, respectively, the second-order macroscopic stress and strain tensors, and σ_i and ε_i, $i=N,L,M$, the stress and strain vectors of the rock mass (the combined system) on a generic microplane. Here, x_i, $i=1,2,3$, are the global Cartesian coordinates and x'_i, $i=N,L,M$, the local Cartesian coordinates of the microplane. In the local coordinates, $n_i, i=1,2,3$, is the unit normal vector of the microplane, and $m_i, l_i, i=1,2,3$, the two orthogonal unit vectors lying within the microplane, see Figure 1(c). The unit vector m_i can be chosen arbitrarily but normal to axis x_3,

$$m_1 = \frac{n_2}{\sqrt{n_1^2+n_2^2}}, m_2 = -\frac{n_1}{\sqrt{n_1^2+n_2^2}}, m_3 = 0 \tag{7}$$

while the other unit vector on the microplane, l_i, can be obtained as the vector product of m_i and n_i, that is, $\boldsymbol{l}=\boldsymbol{m}\times\boldsymbol{n}$.

With the assumption of kinematic constraint in Hypothesis III, the microplane strain vector in the combined system, $\varepsilon_i, i=N,L,M$, is the projection of macroscopic strain tensor ε_{ij},

$$\begin{aligned}&\varepsilon_N = \varepsilon_{ij}N_{ij},\ \ \varepsilon_M = \varepsilon_{ij}M_{ij},\ \ \varepsilon_L = \varepsilon_{ij}L_{ij};\\ &N_{ij} = n_i n_j,\ \ M_{ij} = \frac{1}{2}\left(m_i n_j + m_j n_i\right),\ \ L_{ij} = \frac{1}{2}\left(l_i n_j + l_j n_i\right).\end{aligned} \tag{8a, b, c}$$

The equilibrium between the macroscopic continuum stress and the microplane stresses can be enforced only approximately by a variational principle. This is performed by the principle of virtual work written for the surface of a unit hemisphere Ω [14],

$$\frac{2\pi}{3}\sigma_{ij}\delta\varepsilon_{ij} = \int_{\Omega}(\sigma_N\delta\varepsilon_N + \sigma_M\delta\varepsilon_M + \sigma_L\delta\varepsilon_L)\mathrm{d}\Omega. \tag{9}$$

This leads to the following basic relation between the macrocontinuum stress tensor and the microplane stresses of the rock mass:

DOI: 10.1002/nag

$$\sigma_{ij} = \frac{3}{2\pi}\int_{\Omega} S_{ij}\mathrm{d}\Omega \approx 6\sum_{\mu=1}^{N_m} w_\mu S_{ij}^{(\mu)}, \quad S_{ij} = \sigma_N N_{ij} + \sigma_M M_{ij} + \sigma_L L_{ij} \tag{10a, b}$$

where $S_{ij}^{(\mu)}$ is the contribution of the μ-th microplane to the stress tensor.

5. DAMAGE-BASED MICROPLANE CONSTITUTIVE LAWS OF THE ROCK

5.1. Parallel coupling of the rock matrix and the rock joint

Let $\varepsilon_i^{(R)}, \varepsilon_i^{(J)}$ and $\sigma_i^{(R)}, \sigma_i^{(J)}$ be, respectively, the microplane strain and stress of the rock matrix and the rock joint. According to Hypothesis II, the phases representing the rock matrix and the rock joint are coupled in parallel on the microplane, which means that the strains of the rock matrix and the rock joint are the same as those of the rock mass,

$$\varepsilon_i = \varepsilon_i{}^{(R)} = \varepsilon_i{}^{(J)}, i = N, L, M \tag{11}$$

while the microplane stress of the rock mass is a sum of the stresses in the rock matrix and the rock joint weighted by their fraction in the combined system, that is,

$$\sigma_i = (1-\omega)\sigma_i^{(R)} + \omega\sigma_i^{(J)}, i = N, L, M. \tag{12}$$

We assume that the aforementioned parallel coupling of the rock and joint phases on the microplanes holds for both the elastic and inelastic response of the material. To establish the microplane constitutive law for the combined system, the constitutive laws of these two phases and the evolution law of the joint continuity factor are required.

5.2. Elastic behavior of the rock matrix and the rock joint

Let $E_N^{(K)}, E_T^{(K)}, K = R, J$ be the normal and shear stiffness constants of the rock matrix or the rock joint, respectively, and let $E^{(K)}$ and $v^{(K)}, K = R, J$ be Young's modulus and Poisson's ratio of the intact rock or the joint material on the macrolevel. For a kinematic constraint, the microplane elastic stiffness constants can be linked to the elastic constants of the macrocontinuum [28]:

$$E_N{}^{(K)} = \frac{E^{(K)}}{1-2v^{(K)}}, \quad E_T{}^{(K)} = E_N{}^{(K)}\frac{1-4v^{(K)}}{1+v^{(K)}}, \quad K = R, J. \tag{13a, b}$$

To guarantee nonnegative value for $E_N{}^{(K)}$ and $E_T{}^{(K)}$, only Poisson's ratios in the range 0 to 0.25 can be reproduced, which is sufficient for many intact rocks and rock joints. For intact rock whose v is between 0.25 and 0.5, such as shale and schist, remedy can be made by coupling the rock matrix in series with an isotropic shear-deformable volumetrically rigid element, see Bažant and Oh [11] and Caner and Bažant [13].

For given increments of the microplane strains $\Delta\varepsilon_N^{(K)}$, $\Delta\varepsilon_L^{(K)}$, and $\Delta\varepsilon_M^{(K)}$, $K = R, J$, the elastic parts of the normal and shear stresses of the rock matrix and the rock joint are

$$\begin{aligned}
\sigma_N^{e}{}^{(K)} &= \sigma_N^{o}{}^{(K)} + E_N{}^{(K)}\Delta\varepsilon_N{}^{(K)}, \\
\sigma_L^{e}{}^{(K)} &= \sigma_L^{o}{}^{(K)} + E_T{}^{(K)}\Delta\varepsilon_L{}^{(K)}, \\
\sigma_M^{e}{}^{(K)} &= \sigma_M^{o}{}^{(K)} + E_T{}^{(K)}\Delta\varepsilon_M{}^{(K)}, K = R, J
\end{aligned} \tag{14a, b, c}$$

where $\sigma_N^{o}{}^{(K)}$, $\sigma_L^{o(K)}$, and $\sigma_M^{o}{}^{(K)}$ are the stored previous microplane normal stress and shear stresses in the L-directions and M-directions, respectively.

DOI: 10.1002/nag

The elastic part of the resultant microplane shear stress of the rock matrix or the rock joint is

$$\sigma_T^{e\,(K)} = \sqrt{\left(\sigma_L^{e\,(K)}\right)^2 + \left(\sigma_M^{e\,(K)}\right)^2}, K = R, J. \tag{15}$$

5.3. *Inelastic behavior of the rock matrix and the rock joint*

The inelastic behaviors of the rock matrix and the rock joint can be described by their stress–strain boundaries, which are similar to strain-dependent yield limits. Within the boundaries, the response is assumed to be linear elastic. The advantage of the stress–strain boundary concept is that several independent boundaries for different stress components can be defined as functions of different strain components. If in numerical algorithm the elastic stress components exceed the corresponding stress boundary, the stresses will be dropped to return the boundary at constant stain. At different loading steps, different microplanes will reach the stress–strain boundaries, which cause the macro stress–strain curves to vary their slope gradually.

In recent microplane model M7 for concretes [13], the volumetric–deviatoric split of the elastic strains and of the tensile boundary is abandoned. In this way, previous problems with excessive lateral strains in postpeak extension and with unloading–reloading are now avoided. In M7, the volumetric–deviatoric split is applied only to the compressive boundary, which is split into the volumetric one and the deviatoric one. The volumetric compressive normal stress boundary controls the strain-hardening behavior under high triaxial confining pressure, which never produces softening while the deviatoric compressive normal stress boundary controls the strain-softening behavior when the confinement is weak in at least one direction, as in uniaxial and biaxial compressive loading.

In the present microplane damage model for jointed rock masses, the overall inelastic response of the combined system on microplanes is determined by the inelastic response of the rock phase and joint phase according to their current fraction. The rock matrix is a strain-hardening material that can transmit tensile, compressive, and shear stress on microplanes, while the rock joints are much weaker being able to transmit only compressive and shear stresses on microplanes. The overall strain-softening behavior of the combined system is due to an increase of the fraction of the rock joint phase and to its much lower strength relative to that of the rock phase.

To consider the load carrying capacity of the combined system under different stress conditions, the tensile normal, the compressive normal, and the shear stress–strain boundaries of the rock matrix and the joint may be formulated as follows:

1. Tensile normal stress–strain boundaries of the rock matrix and the rock joint.

The tensile normal stress boundaries of the rock or joint phases limit their respective load carrying capacities on the microplane. Here, constant tensile strength values are used for both the rock matrix and the rock joint:

$$\sigma_N^{b+(R)} = T^{(R)}, \quad \sigma_N^{b+(J)} = T^{(J)} \tag{16a, b}$$

where $T^{(R)}, T^{(J)}$ are the tensile strengths of the rock matrix and the rock joint on the microplane, respectively.

2. Compressive normal stress boundaries of the rock matrix and the rock joint.

The compressive normal stress boundary of the rock matrix approximately reflects the effect of microvoids at low confining pressures, and the strength increases because of confinement. It depends on the normal strain and the volumetric strain as follows:

$$\begin{aligned} &\sigma_N^{b-(R)} = -\alpha T^{(R)}, \\ &\alpha = \alpha_0\left[1 + \left(\left\langle -\varepsilon_N - \varepsilon_N^o \right\rangle / (c_1\xi_1)\right)^{1.5}\right], \ \xi_1 = 1/\left(1 + \tanh\left(\left\langle -\varepsilon_V - \varepsilon_V^o \right\rangle / c_2\right)\right) \end{aligned} \tag{17a, b, c}$$

where α_0 is the ratio of the minimum normal compressive strength to the tensile strength of the rock matrix on the microplane, $\varepsilon_N^o, \varepsilon_V^o$ are the normal strain and volumetric strain thresholds of the rock

DOI: 10.1002/nag

matrix, respectively, and c_1, c_2 are material parameters controlling the dependence of the compressive stress boundary of the rock matrix on normal strain and confinement, respectively.

Due to the waviness of the joint surface, the rock joint cannot entirely close under compression, and so the normal compressive stress cannot be fully transferred. We introduce a variable, β, called the joint mobilization factor, to represent the fraction of compressive strength mobilized by the rock joint. The boundary must characterize the increase of compressive strength of the rock joint during its gradual closing, and also its strength increases because of confinement. This can be accomplished as follows:

$$\sigma_N^{b-(J)} = -\alpha_0 \beta T^{(R)};$$
$$\beta = \beta_c\left(1 - e^{-\xi_2}\right), \quad \xi_2 = \left\{\langle -\varepsilon_N\rangle / [(\varepsilon_{\mathrm{I}}{}^o - \varepsilon_{\mathrm{III}}{}^o) + a]\right\}^{0.5} \tag{18a, b, c}$$

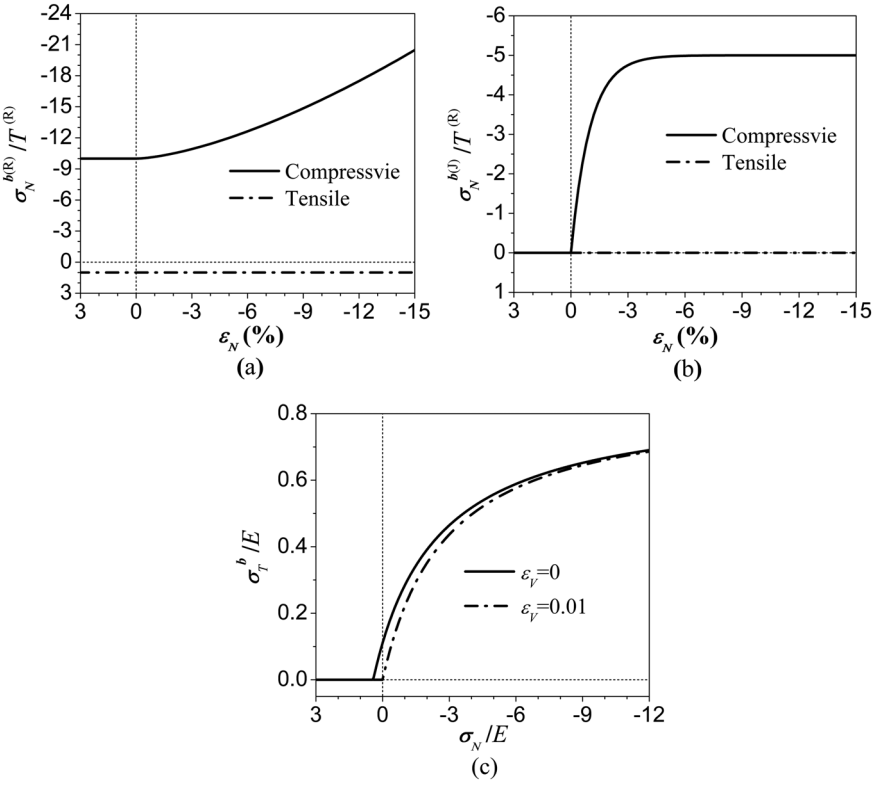

Figure 2. Stress boundaries used in the microplane damage model for rocks: (a) normal stress boundaries of the rock matrix, (b) normal stress boundaries of the rock joint, and (c) shear stress boundary of the rock matrix and the rock joint.

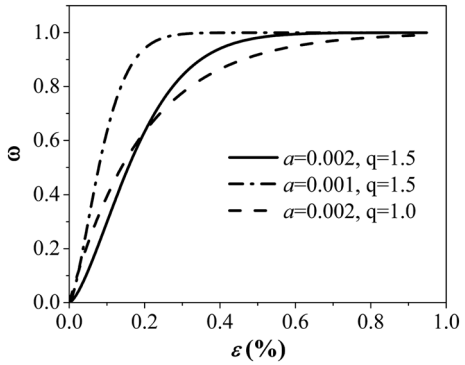

Figure 3. The damage evolution law as exponential function of strain history parameter.

DOI: 10.1002/nag

where β_c is the maximum value of the joint mobilization factor for the compressive normal strength, $\varepsilon_{\mathrm{I}}^o, \varepsilon_{\mathrm{III}}^o$ are the maximum and minimum principal strains at the beginning of the current step, respectively, and a is a very small value introduced to prevent the overflow error in the calculation.

3. Shear stress-strain boundaries of the rock matrix and the rock joint.

In general, the shear strengths of the rock matrix and the rock joint will increase with the negative normal stress and the confinement. Similar shear stress–strain boundaries as in microplane models M4 [12] and M7 [13] for concrete are adopted here for the rock matrix and the rock joint:

$$\sigma_T^{b(K)} = \frac{E'_T{}^{(K)} c_3 \left\langle \widehat{\sigma}_N^{o(K)} - \sigma_N{}^{(K)} \right\rangle}{E'_T{}^{(K)} + c_3 \left\langle \widehat{\sigma}_N^{o(K)} - \sigma_N{}^{(K)} \right\rangle}, \qquad \widehat{\sigma}_N^{o(K)} = E'_T{}^{(K)} c_4 \left\langle 1 - \langle \varepsilon_V \rangle / \varepsilon_V^o \right\rangle, \quad E'_T{}^{(K)} = E^{(K)} / \left(1 + \nu^{(K)}\right), K = R, J \tag{19a, b, c}$$

in which c_3 and c_4 are material parameters that control the dependence of shear stress–strain boundary on the normal stress and on the confinement, respectively, and $\sigma_N^o(R), \sigma_N^o(J)$ are the normal stress thresholds of the rock matrix and the rock joint, respectively.

Because the volumetric strain is the average of the normal strains on all microplanes, the dependence of stress–strain boundaries on the volumetric strain in the formulation implies the interaction between microplanes of various orientations.

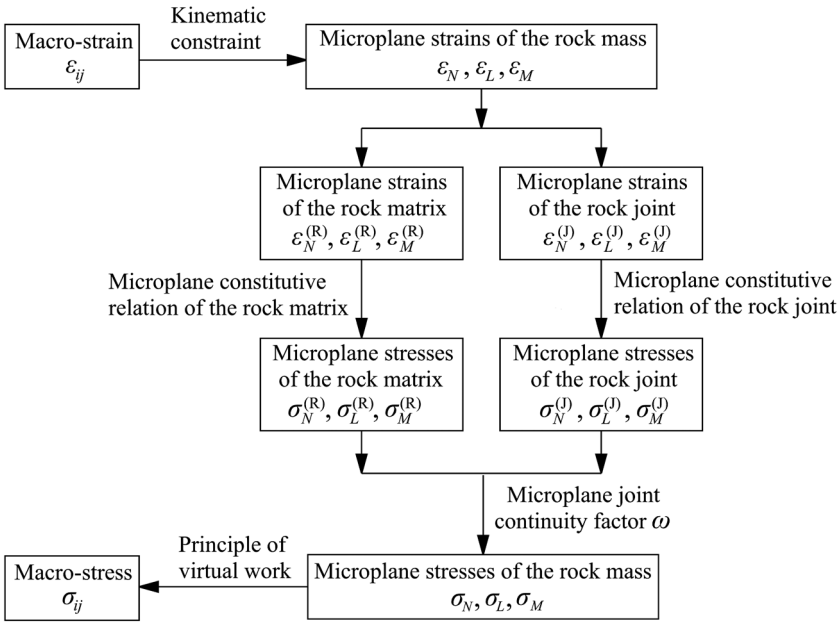

Figure 4. The flow of calculation between the macrolevel and microlevel with parallel coupling of the two phases on microplane.

Table I. The unit normal vector and the plane dip angle of microplanes $\mu = 3$, 17, 7, 15, and 1.

μ	n_1^α	n_2^α	n_3^α	θ (°)
3	0	0	1	0
17	0.30895127	0	−0.9510779	18
7	0.70710678	0	−0.7071068	45
15	0.95107787	0	−0.3089513	72
1	1	0	0	90

DOI: 10.1002/nag

With the following parameter values $\alpha_0 = 10$, $\beta_c = 0.5$, $\varepsilon_N^o = 0.0005$, $\varepsilon_V^o = 0.001$, $c_1 = 0.2$, $c_2 = 0.005$, $c_3 = 0.3$, and $c_4 = 0.5$, the basic features of the normal and shear stress–strain boundaries of the rock matrix and the rock joint are shown in Figure 2.

In the explicit computational algorithm, the elastic moduli are used in every time step to obtain the elastic stress increment. If the stress point exceeds the stress–strain boundary, the stress is dropped vertically (at constant strain) to the boundary, which constitutes the inelastic stress increment. The drop of microplane normal stress thus occurs at constant microplane strain; then, the drop of shear stress occurs at constant updated normal stress. This is achieved by the equations:

$$\sigma_N^{f\,(K)} = \max\left(\min\left(\sigma_N^{e\,(K)}, \sigma_N^{b+(K)}\right), \sigma_N^{b-(K)}\right), \quad K = R, J. \tag{20}$$

$$\sigma_T^{f\,(K)} = \min\left\{\sigma_T^{e\,(K)}, \sigma_T^{b\,(K)}\right\}, \quad K = R, J. \tag{21}$$

The final shear stress components in the coordinates of the microplane, $\sigma_L^{f\,(K)}, \sigma_M^{f\,(K)}, K = R, J$ are calculated under the assumption of proportionality to their corresponding elastic stress components:

$$\sigma_L^{f\,(K)} = \sigma_T^{f\,(K)} \sigma_L^{e\,(K)} / \sigma_T^{e\,(K)}, \quad \sigma_M^{f\,(K)} = \sigma_T^{f\,(K)} \sigma_M^{e\,(K)} / \sigma_T^{e\,(K)}, \quad K = R, J. \tag{22a, b}$$

Table II. Material parameters used for the sandstone.

Parameter	Meaning	Value
$E^{(R)}$	Young's modulus of the rock matrix	25 GPa
$E^{(J)}$	Young's modulus of the rock joint	25 GPa
$\nu^{(R)}$	Poisson's ratio of the rock matrix	0.18
$\nu^{(J)}$	Poisson's ratio of the rock joint	0.18
$T^{(R)}$	Microplane tensile strength of the rock matrix	50 MPa
$T^{(J)}$	Microplane tensile strength of the rock joint	0
α_0	The ratio of the minimum microplane normal compressive strength to the microplane tensile strength of the rock matrix	10
β_c	The maximum value of the joint mobilization factor for normal compressive strength of the rock joint	0.5
$\varepsilon^0{}_V$	The volumetric strain threshold of the rock matrix	0.001
$\varepsilon^0{}_N$	The normal strain threshold of the rock matrix	0.0005
c_1	Controls dependence of compressive normal stress boundary of the rock matrix on normal strain	0.2
c_2	Controls dependence of compressive normal stress boundary of the rock matrix on volumetric strain	0.005
c_3	Controls dependence of shear stress boundary on the normal stress	0.001
c_4	Controls dependence of shear stress boundary on the confinement	0.05
a_1	Controls dependence of damage evolution on historic maximum positive volumetric strain	0.002
a_2	Controls dependence of damage evolution on historic maximum positive deviatoric strain	0.0025
a_3	Controls dependence of damage evolution on historic maximum shear strain	0.05
q_1	Controls rate of damage evolution related to historic maximum positive volumetric strain	1.5
q_2	Controls rate of damage evolution related to historic maximum positive deviatoric strain	1.5
q_3	Controls rate of damage evolution related to historic maximum shear strain	1

DOI: 10.1002/nag

5.4. *Evolution law of the joint continuity factor*

The nonlinear inelastic behavior of the rock originates not only in the rock matrix but also, and mainly, in the rock joint. The evolution of the rock joint may be described by the joint continuity factor, which characterizes the cracking process in the rock matrix. It is generally known that, under unconfined compression, the rock tends to fail by longitudinal splitting fracture. At moderate lateral confining pressure, the splitting fracturing tends to be suppressed, and the rock fails along an inclined plane of compression–shear. At high enough confining pressure, the rock becomes rather ductile, and the failure occurs through a network of many small shear fractures. Under uniaxial tension, a tensile mode I fracture perpendicular to the loading direction typically appears.

Different mechanisms can be discerned in the damage evolution. Under low confinement compression, and also under uniaxial tension, the initiation and propagation of opening mode cracks are accompanied by accumulation of volumetric expansion and positive deviatoric strains. When the shear stress along the microplane is high, shear cracking proceeds along that plane.

The damage evolution is mainly controlled by the maximum positive values of the volumetric strain, deviatoric strain, and shear strain reached so far on the microplanes. Denoting them as ε_V^{+h}, $\varepsilon_D^{+h}, \varepsilon_T^h$, respectively, one can describe the damage evolution by decaying exponentials of power laws [3, 7]:

$$\omega = 1 - e^{-\left[\left(\varepsilon_V^{+h}/a_1\right)^{q_1} + \left(\varepsilon_D^{+h}/a_2\right)^{q_2} + \left(\varepsilon_T^h/a_3\right)^{q_3}\right]} \tag{23}$$

where a_1, a_2, a_3 and q_1, q_2, q_3 are empirical material parameters; $\varepsilon_D = \varepsilon_N - \varepsilon_V$ is the deviatoric strain.

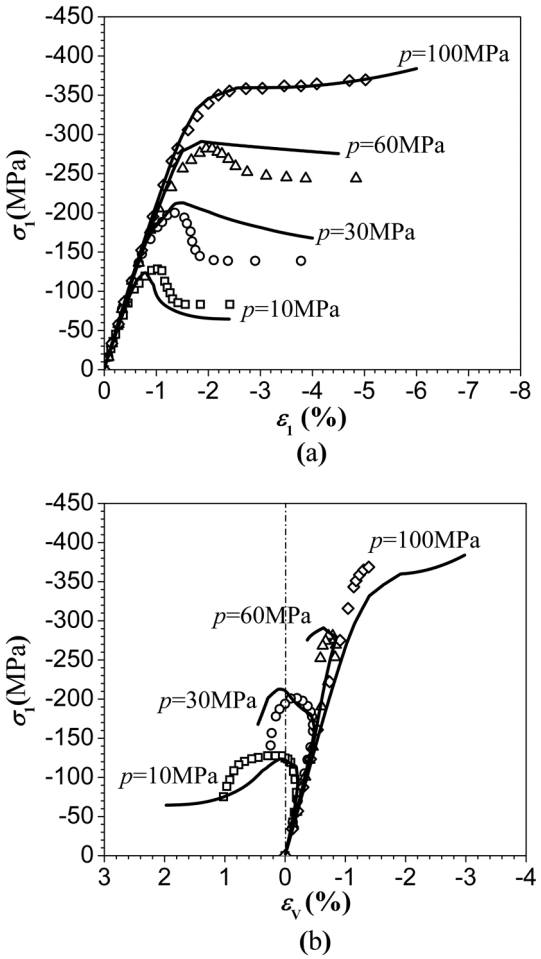

Figure 5. Simulation of the triaxial test of the sandstone from Southwest Germany by Gowd and Rummel [29]: (a) axial stress versus axial strain and(b) axial stress versus volumetric strain.

DOI: 10.1002/nag

Figure 3 gives an example of material damage evolution with increasing strain at different parameters a, q according to the function $\omega = 1 - e^{-(\varepsilon/a)^q}$.

6. CALIBRATION AND COMPARISON WITH THE TEST DATA

The present microplane damage model for rock was implemented in a FORTRAN material subroutine for a finite element program. The flow of calculation between the macrolevel and microlevel with parallel coupling of the two phases on microplane is explained in Figure 4. The optimal Gaussian integration formula for the surface of a unit sphere with $N_m = 37$ integration points per hemisphere (derived in [11]) was used to integrate the stress tensor from the stresses on 37 microplanes normal to the radial vectors at these points. For the sake of illustration, we will later consider the dip angle of the microplane, θ, defined as the angle between the microplane and axis x_1 in the global Cartesian coordinates $ox_1x_2x_3$. It will be convenient to consider microplanes $\mu = 3$, 17, 7, 15, and 1, whose unit normal vectors are perpendicular to the axis x_2. Their dip angles are 0°, 18°, 45°,72°, and 90°, respectively, as listed in Table I along with their unit vector coordinates.

To calibrate and verify the model, simulations were run to optimally fit the triaxial compression test data for sandstone from Southwest Germany, as reported by Gowd and Rummel [29], and the uniaxial compression test data for a jointed plaster mortar, as reported by Kawamoto *et al*. [4] (the test results are shown in all the figures by circle points and the model predictions by continuous curves). For simplicity, it was assumed in the simulations that Young's modulus and Poisson's ratio of the rock joint are equal to those of the rock matrix, that is, $E^{(J)} = E^{(R)}$, $\nu^{(J)} = \nu^{(R)}$.

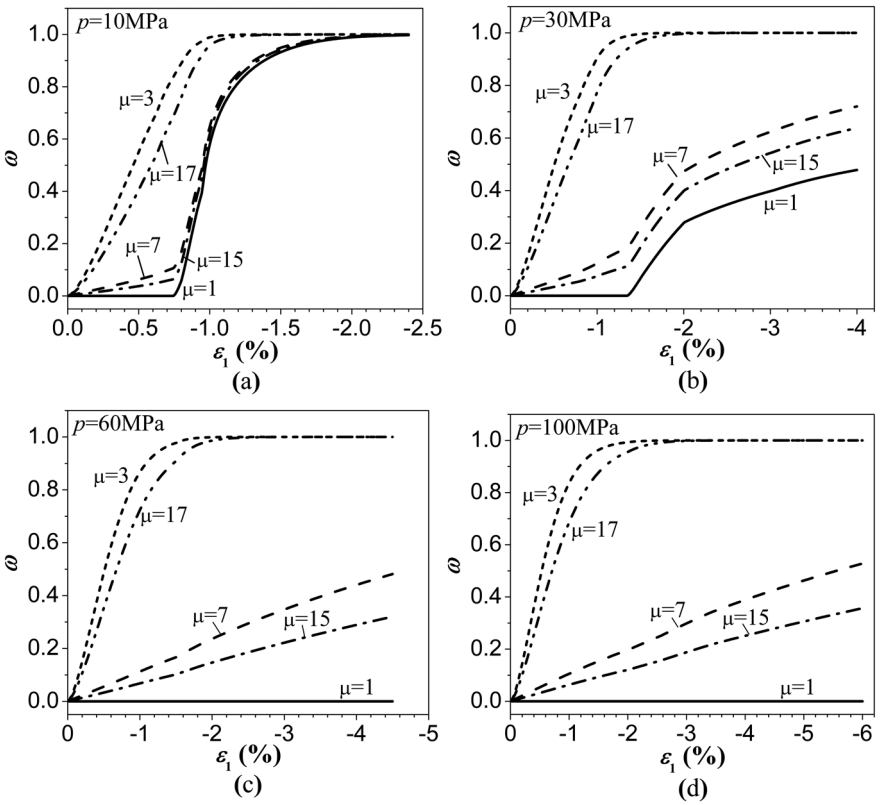

Figure 6. The joint continuity factor on microplane versus axial strain: (a) $p = 10$ MPa, (b) $p = 30$ MPa, (c) $p = 60$ MPa, and (d) $p = 100$ MPa.

DOI: 10.1002/nag

6.1. Numerical results for a sandstone under triaxial compression

The triaxial compression test of the sandstone by Gowd and Rummel [29] was simulated. The sandstone taken from SW-Germany was a medium grain sized with subangular to round quartz grains bedded within a clayey matrix. Below a critical value of axial stress, the rock deformed linearly and elastically. Further compression led to inelastic deformation. The transition from brittle to ductile deformation occurred at about confining pressure 90 MPa.

The simulation led to the material parameters listed in Table II, in which the meaning of each parameter is briefly indicated.

The curves of the axial stress versus the axial strain and the volumetric strain at confining pressures 10, 30, 60, and 100 MPa are plotted in Figure 5. The curves document that the model can characterize the main features of standard triaxial compression tests of intact rock. At low or medium pressures $p = 10$, 30, and 60 MPa, the stress–strain curves show strain softening and dilatancy, namely, an inelastic expansion relative to the elastic compression in volumetric deformation. The transition from brittle to ductile deformation takes place at confining pressure $p = 100$ MPa, marked by strain hardening and absence of dilatancy. With increasing confinement, the predicted strength increases while volumetric expansion decreases, as exhibited in the experiments.

For illustration, we consider microplanes $\mu = 3$, 17, 7, 15, and 1. The curves of the joint continuity factors versus axial strain at different confining pressure are depicted in Figure 6. As can be seen, the microplane damage at the same axial strain decreases with the microplane dip angle. As the confinement increases, the growth of damage on the microplanes gets gradually suppressed as the dip angle becomes higher ($\mu = 7$, 15, and 1).

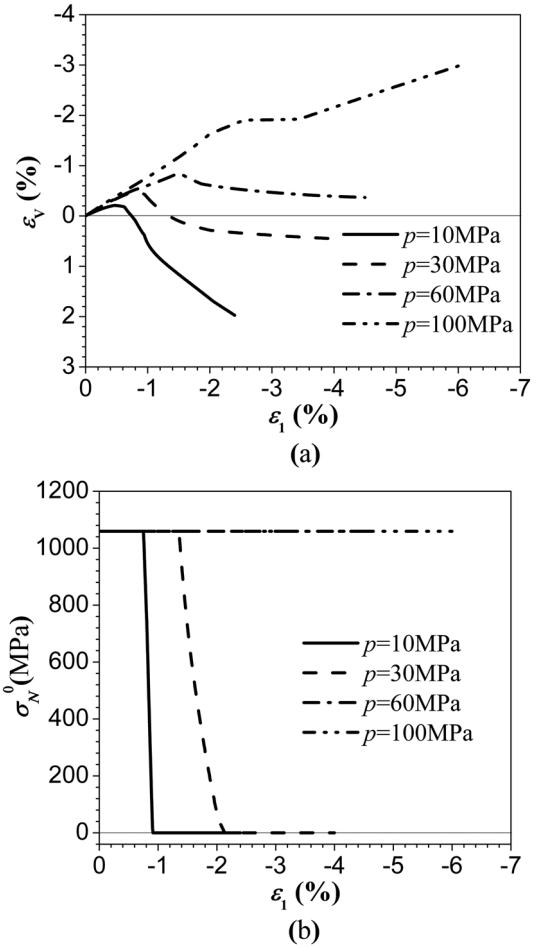

Figure 7. (a) The volumetric strain versus axial strain and (b) normal stress threshold versus axial strain.

DOI: 10.1002/nag

To clarify the dependence of the stress–strain boundaries on the confinement, Figure 7 depicts the variation of the volumetric strain and the normal stress thresholds with the axial strain. In the simulations, due to the same value of the Young's modulus and Poisson's ratio, the normal stress threshold of the rock matrix equals that of the rock joint. For the shear stress boundaries, the contribution of the normal stress threshold and the normal stress can be related to the two different mechanisms, that is, the cohesion mechanism and the friction mechanism, respectively. Figure 7(b) shows the model to capture the decrease of cohesion with increasing axial strain at the confining pressure of $p = 10$ and 30 MPa, which is due to volume expansion at low confinement.

To illustrate how the microplane response of the combined system depends on the two phases, the rock matrix and the joint, the strains, and stresses on microplanes $\mu = 1$, 3, and 7 may be investigated. The shear strains on the microplanes $\mu = 1$ and 3 are nearly zero. Figure 8 plots the normal strains on microplanes $\mu = 1$ and 3 versus the axial strain. Figure 9 plots the normal and shear strains on microplane $\mu = 7$ versus the axial strain. As one can see, except for shear strain on microplane $\mu = 7$ at the confining pressure of $p = 10$ MPa, normal strains and shear strains on these microplanes increase with the axial strain.

Figures 10–12 and Figure 13 plot the normal stress and the shear stress, respectively, versus the axial strain as exhibited by the rock matrix, the rock joint, and the combined system of microplanes $\mu = 1$, 3, and 7. For microplane $\mu = 1$, the normal stresses of the combined system and the two phases, rock matrix and joints, are compressive. The strain softening exhibited by the normal stress of the combined system under lower confining pressures may be attributed both to a lower compressive strength of the rock joint and to a gradual increase in the rock joint fraction. Under

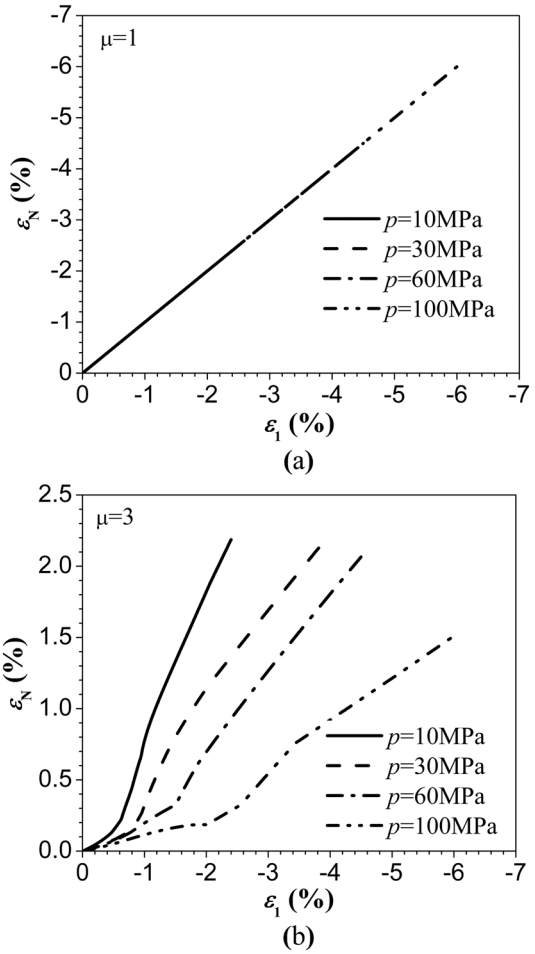

Figure 8. The normal strain versus axial strain on microplanes: (a) $\mu = 1$ and (b) $\mu = 3$.

DOI: 10.1002/nag

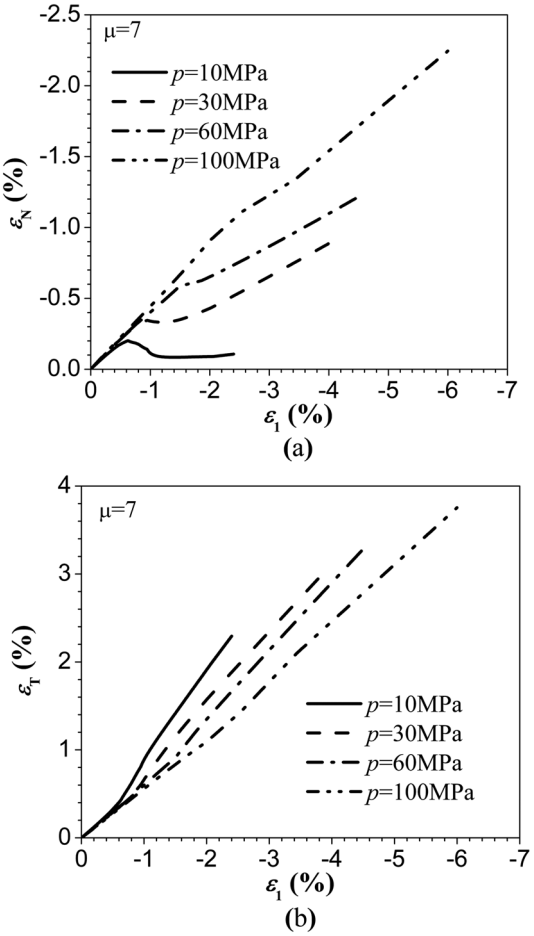

Figure 9. The strains on the microplane $\mu = 7$ versus axial strain (a) the normal strain and (b) the shear strain.

higher confining pressures, the strain-hardening behavior of the combined system may be explained by suppressed microplane damage growth and by strain-hardening response of the rock matrix.

For microplane $\mu = 3$, the tensile normal stress of the combined system exhibits strain-softening behavior at any confining pressure. Doubtless this is due to fast microplane damage growth at vanishing tensile strength of the rock joint.

For microplane $\mu = 7$, the normal stresses of the combined system under confining pressures $p = 10$ MPa and $p = 100$ MPa exhibit strain softening, while they show strain hardening under confining pressures $p = 30$ MPa and $p = 60$ MPa. The shear stresses of the combined system under confining pressure $p = 10$ MPa and $p = 30$ MPa first increase with the axial strain but then decrease fast to a very low value, while under confining pressures $p = 60$ MPa and $p = 100$ MPa, they first increase then keep nearly constant. The decrease of the shear stress of the combined system under confining pressure $p = 30$ MPa may be explained by the dominance of the cohesion mechanism over the friction mechanism.

6.2. *Numerical results for a jointed plaster mortar under uniaxial compression*

The optimum fitting of Kawamoto *et al.*'s [4] data on the anisotropic behavior of a uniaxially compressed plaster mortar with one set of parallel open joints led to the material parameters values listed in Table III, in which $\varepsilon_N^o, \varepsilon_V^o, c_2, c_3, c_4, a_1, q_1, q_2, q_3$ take the same values as for the sandstone. Here, in view of the low compressive normal strength of the preexisting open joints, the maximum value of the joint mobilization factor, β_c, is set to a very small value, 0.01.

Consider first the specimen with one set of joints, and denote the local Cartesian coordinates of the joint plane as $ox'_1x'_2x'_3$. Axis x'_1 is chosen to be parallel to the normal of the joint plane, and axis x'_2 is chosen

DOI: 10.1002/nag

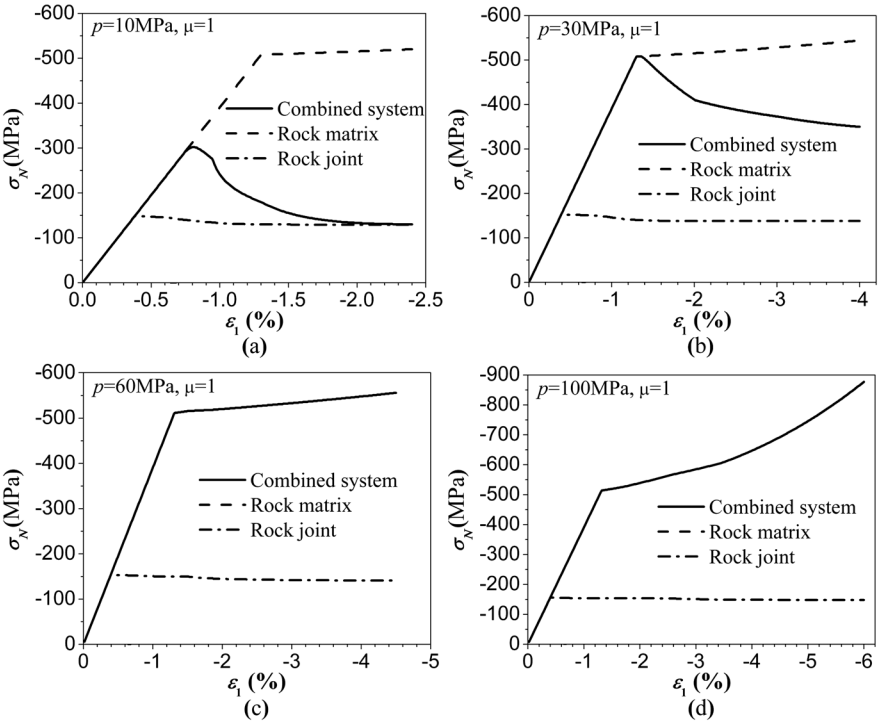

Figure 10. The normal stress on the microplane $\mu = 1$ versus axial strain: (a) $p = 10$ MPa, (b) $p = 30$ MPa, (c) $p = 60$ MPa, and (d) $p = 100$ MPa.

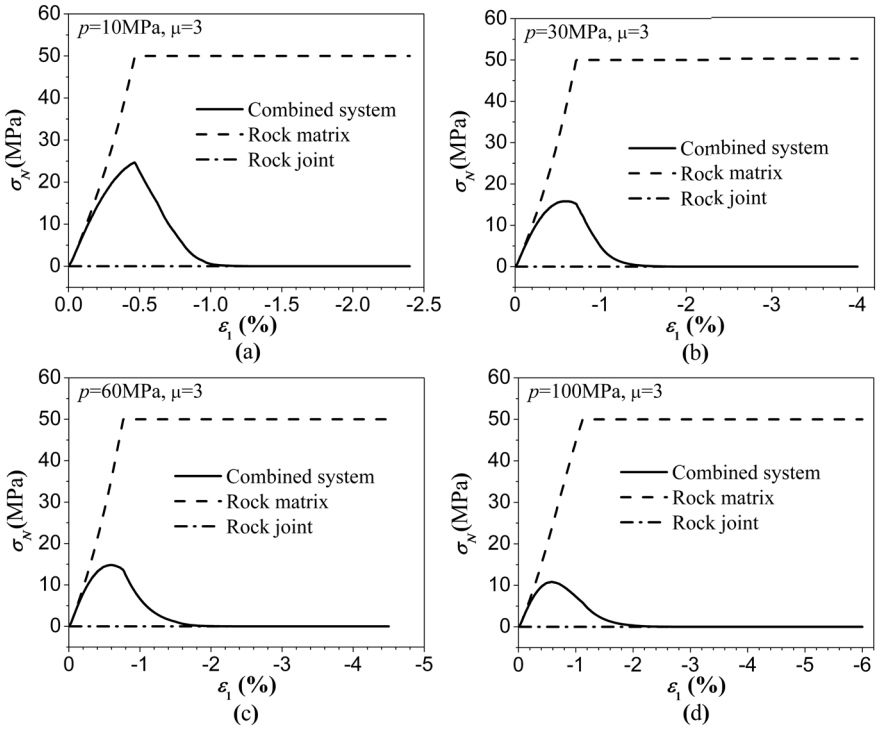

Figure 11. The normal stress on the microplane $\mu = 3$ versus axial strain: (a) $p = 10$ MPa, (b) $p = 30$ MPa, (c) $p = 60$ MPa, and (d) $p = 100$ MPa.

DOI: 10.1002/nag

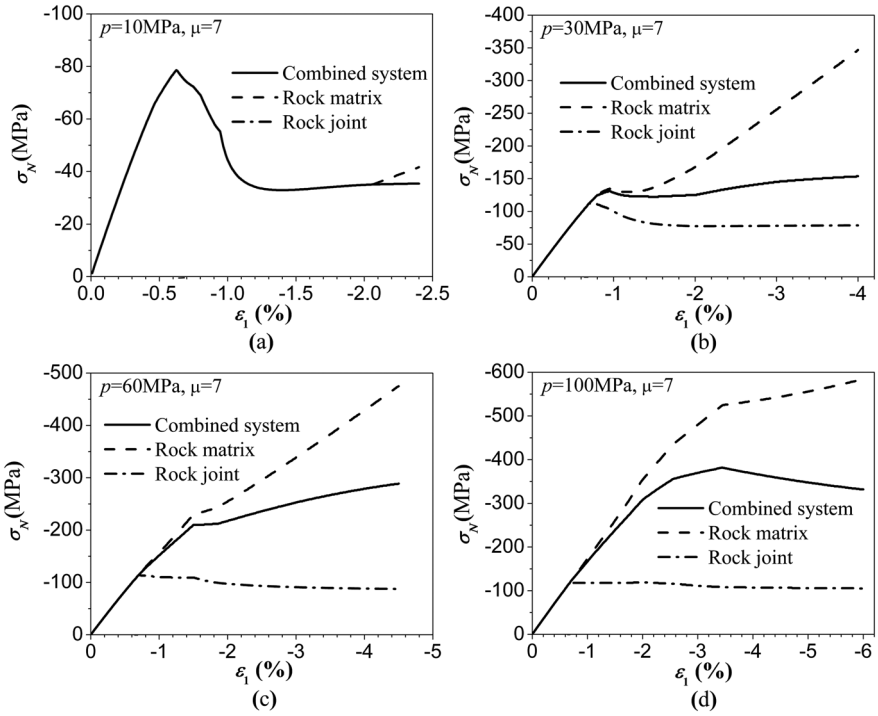

Figure 12. The normal stress on the microplane $\mu = 7$ versus axial strain: (a) $p = 10$ MPa, (b) $p = 30$ MPa, (c) $p = 60$ MPa, and (d) $p = 100$ MPa.

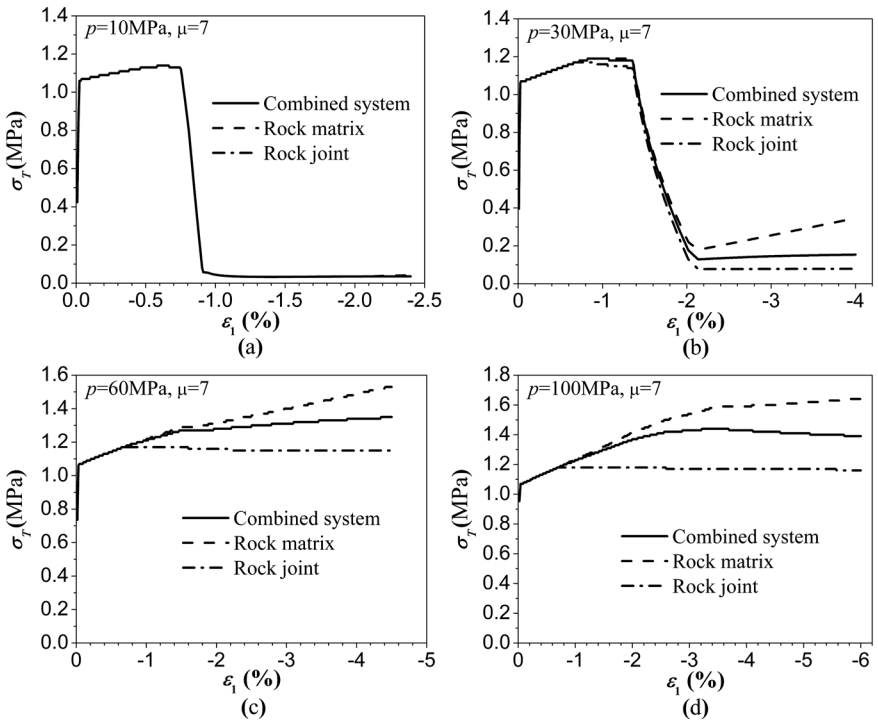

Figure 13. The shear stress on the microplane $\mu = 7$ versus axial strain: (a) $p = 10$ MPa, (b) $p = 30$ MPa, (c) $p = 60$ MPa, and (d) $p = 100$ MPa.

DOI: 10.1002/nag

to coincide with axis x_2 of the global Cartesian coordinates $ox_1x_2x_3$. The joint plane dip angle θ_j is defined as the angle between the joint planes and the axial stress σ_1 or the axis x_1. For the joint continuity factor, the second-order fabric tensor of the second kind may be written in the local coordinates, ρ'_{ij}, as

$$\rho'_{ij} = \begin{bmatrix} \omega_0 & 0 & 0 \\ 0 & 0 & 0 \\ 0 & 0 & 0 \end{bmatrix} \tag{24}$$

where ω_0 is the initial value of the joint continuity factor on the joint plane before loading.

Table III. Material parameters used for the jointed plaster mortar.

$E^{(R)}$ (MPa)	$E^{(J)}$ (MPa)	$\nu^{(R)}$	$\nu^{(J)}$	$T^{(R)}$ (MPa)	$T^{(J)}$ (MPa)		
1110	1110	0.17	0.17	0.5	0		
α_0	β_c	$\varepsilon^0{}_V$	$\varepsilon^0{}_N$	c_1	c_2	c_3	c_4
5	0.01	0.001	0.0005	0.15	0.005	0.001	0.05
a_1	a_2	a_3	q_1	q_2	q_3		
0.002	0.001	0.025	1.5	1.5	1		

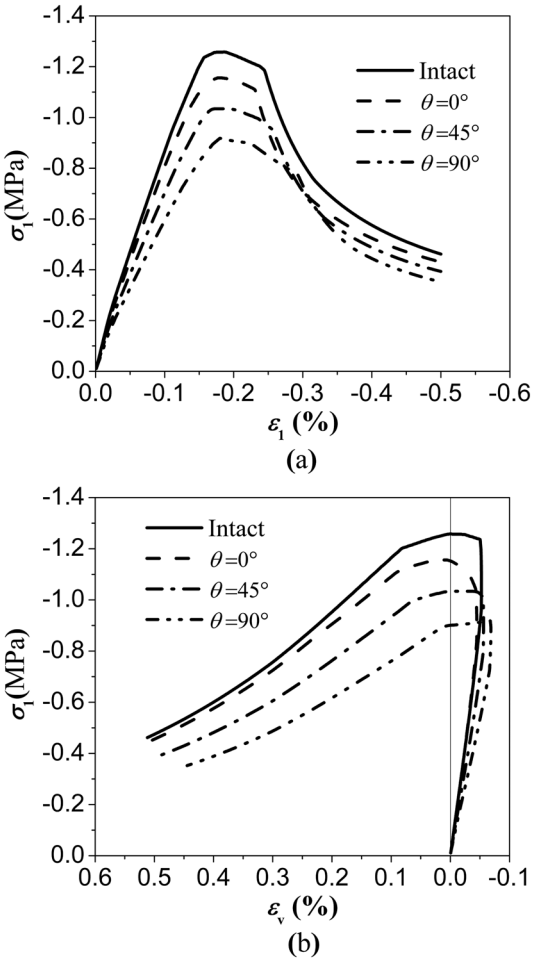

Figure 14. The numerical results for the intact and jointed plaster mortar specimens under uniaxial compression: (a) axial stress versus axial strain and (b) axial stress versus volumetric strain.

DOI: 10.1002/nag

For simplicity, the joint continuity factor for a penetrating joint is defined as the ratio of the length of the joint to the combined length of the joint and the rock bridges [30]. Thus, the value of ω_0 for the plaster mortar is 0.45.

With the second kind of fabric tensor, the joint continuity factor on each microplane can be approximated by

$$\omega^{(\mu)}(\mathbf{n}) \approx \rho'_{ij} n'^{(\mu)}_i n'^{(\mu)}_j. \tag{25}$$

The uniaxial compression tests of the intact specimen and of the jointed specimens with different joint plane angles are simulated. Figure 14 plots the curves of the axial stress versus the axial strain and the volumetric strain. The peak strengths and Young's moduli of the jointed specimens are normalized by those of the intact specimen. Figure 15 presents a comparison of the test results with the unified strength and unified Young's modulus predicted by the model for the jointed plaster mortar. For specimens with joint plane dip angles $\theta_j = 0°, 45°, 90°$, Figure 16 shows the growth of the joint continuity factor with axial strain on the microplanes $\mu = 1$, 3, and 7.

As can be seen, the predicted stress–strain curves exhibit strain softening and dilatancy for the intact as well as the jointed specimens. The predicted unified strengths and Young's moduli of the jointed specimen decrease with the joint dip angle, which agrees with the test results.

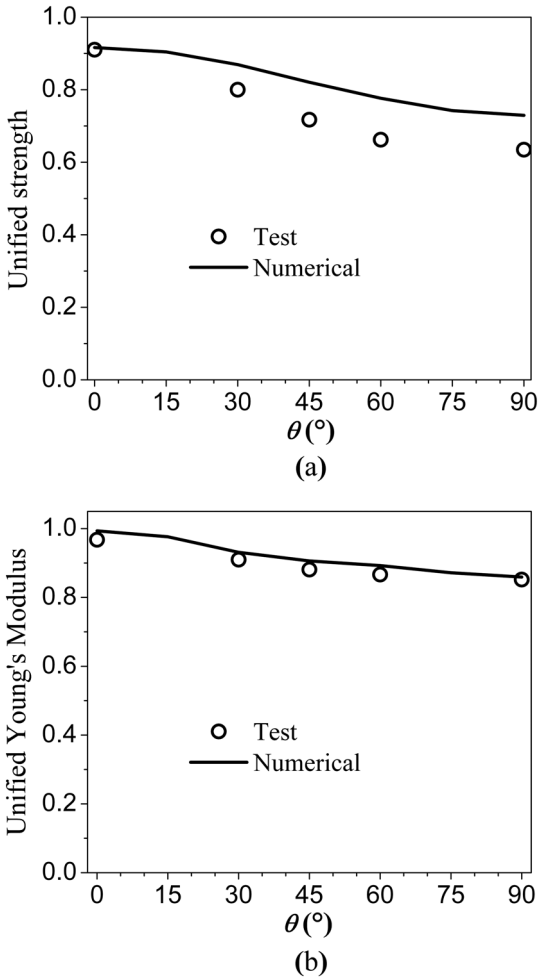

Figure 15. (a) Unified strength and (b) unified Young's moduli versus joint dip angle for the plaster mortar specimen.

DOI: 10.1002/nag

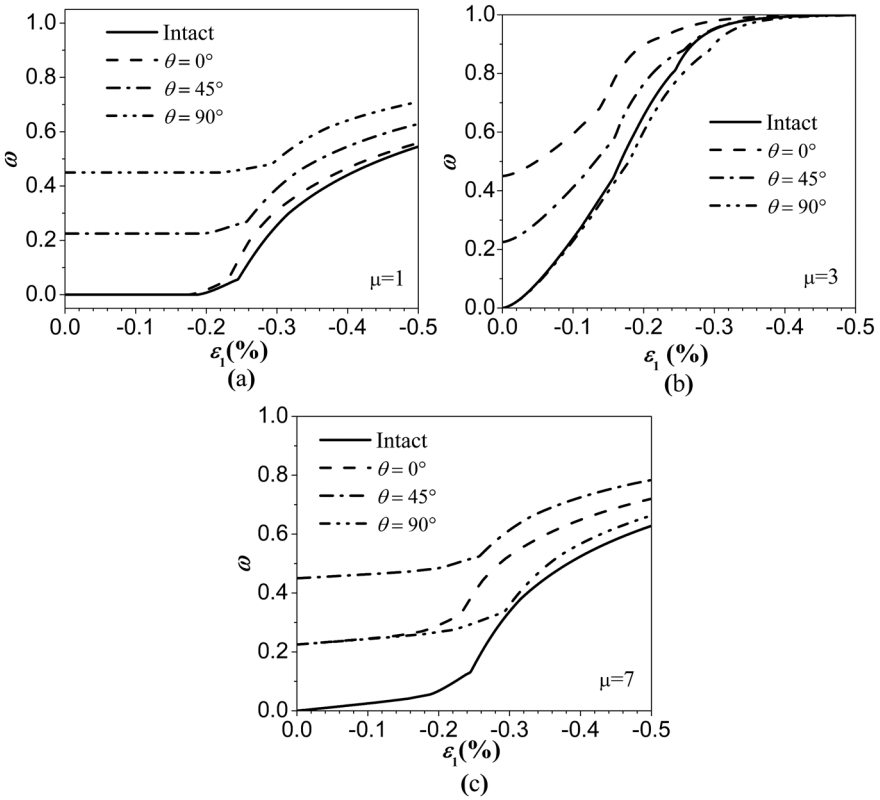

Figure 16. The joint continuity factor on microplanes (a) $\mu = 1$ and (b) $\mu = 3$ versus axial strain for the plaster mortar specimen.

Thesimulation of the anisotropic behavior of the jointed specimen is controlled by the initial value and evolution of the joint continuity factor, the dip angle of the joint plane with regard to the loading direction, and the nonlinear response of the rock and the joint. The less satisfactory agreement of strengths than those of elastic moduli may be caused by the sensitivity of the former to the other geometrical parameters of the joints, such as spacing and arrangement patterns.

In the proposed microplane damage model for jointed rock masses, there are 20 material parameters to be identified. They include (i) the elastic parameters of the rock matrix and the rock joint, $E^{(R)}$, $\nu^{(R)}$, $E^{(J)}$, and $\nu^{(J)}$; (ii) the microplane strength parameters of the rock matrix and the rock joint, $T^{(R)}$, $T^{(J)}$, α_0, β_c, ε_N^o, ε_V^o, c_1, c_2, c_3, and c_4; and (iii) the damage evolution parameters of the rock matrix, a_1, q_1, a_2, q_2, a_3,and q_3. For a given rock mass, the elastic parameters can first be estimated through the elastic behavior of the intact rock and the filling material of the rock joint. Because the microplane strength parameters $\varepsilon_N^o, \varepsilon_V^o, c_1, c_2, c_3, c_4$ and the damage evolution parameters $a_1, q_1, a_2, q_2, a_3, q_3$ mainly control the shape of the nonlinear stress–strain curve, they can be set the same value for a certain type of rocks. Finally, the remaining strength parameters $T^{(R)}$, $T^{(J)}$, α_0, and β_c can be obtained from optimal fitting to the strengths of the intact rock or the rock mass under different confining pressure. For jointed rock mass, the most difficult part in the calibration is the formulation of the microplane damage variable as a function of the geological data of joint sets, such as persistence, spacing, and arrangement pattern. It is generally recognized that joint persistence plays the most important role among others in the failure process of the rock mass. However, to consider the influence of the other geometrical parameters in general, further experiment study is required.

As shown in these simulations, with only 37 integration points, the model can obtain a reasonable result in a nonlinear incremental analysis. The procedure of implementation in finite element analyses is the same as other microplane models; the basic flowchart can be found in Carol *et al.*[31].

DOI: 10.1002/nag

7. CONCLUSIONS

1. The main conclusion is that, in order to describe with the microplane model the nonlinear damage behavior of jointed rock under general traixial loading, including compression, the isotropic rock matrix, and the joints (or cracks), may be considered as two distinct phases that are coupled in parallel (and thus undergo equal overall strains).
2. The inelastic softening behavior can be realistically modeled by introducing the joint continuity factor as the stress-carrying area fraction. Thus, the model can consider the independent influence of the geometrical parameters and the mechanical response of discontinuities in rocks.
3. The optimized numerical simulations presented document satisfactory fits of previously published triaxial test data on sandstone—an intact rock, without joints. The fits reproduce the essential features such as the strain softening and dilatancy under low confining pressure, as well as the brittle–ductile transition under higher confining pressure.
4. The optimal fitting of previously published data on jointed plaster mortar shows that the salient features such as the decrease of jointed rock strength and of Young's modulus with an increasing dip angle of the joint can be realistically reproduced.

ACKNOWLEDGEMENTS

The work presented here was supported by the National Science Foundation of China (NSFC) under grant no. 11102224 and by the Fundamental Research Funds for the Central Universities of China under grant no. 2009QL05. The work of the second author was supported by the US National Science Foundation under grant no. CMMI-1153494 to Northwestern University, which also provided the facilities for the conduct of research.

REFERENCES

1. Bieniawski ZT. The effect of specimen size on compressive strength of coal. *International Journal of Rock Mechanics and Mining Sciences & Geomechanics Abstracts* 1968; **5**(4):325–335.
2. Dragon A, Mroz Z. A continuum model for plastic brittle behavior of rock and concrete. *International Journal of Engineering Science* 1979; **17**(2):121–137.
3. Frantziskonis G, Desai CS. Elastoplastic model with damage for strain softening geomaterials. *Acta Mechanica* 1987; **68**(3/4):151–170.
4. Kawamoto T, Ichikawa Y, Kyoya T. Deformation and fracturing behavior of discontinuous rock mass and damage mechanics theory. *International Journal for Numerical and Analytical Methods in Geomechanics* 1988; **12**(1):1–30.
5. Kachanov LM. Time of the rupture process under creep conditions. *Izv Akad Nauk SSR, Otd Tekh Nauk* 1958; **8**:26–31.
6. Rabotnov IN. On the equations of state for creep. *Progress in Applied Mechanics-The Prager Anniversary* 1963; **8**:307–315.
7. Carol I, Bažant ZP, Prat PC. Geometric damage tensor based on microplane model. *Journal of Engineering Mechanics, ASCE* 1991; **117**(10):2429–2448.
8. Lemaitre J, Desmorat R, Sauzay M. Anisotropic damage law of evolution. *European Journal of Mechanics A-Solids* 2000; **19**(2):187–208.
9. Brocca M, Bažant ZP. Microplane constitutive model and metal plasticity. *Applied Mechanics Reviews, ASME* 2000; **53**(10):265–281.
10. Caner FC, Bažant ZP, Červenka J. Vertex effect in strain-softening concrete at rotating principal axes. *Journal of Engineering. Mechanics, ASCE* 2002; **128**(1):24–33.
11. Bažant ZP, Oh BH. Microplane model for progressive fracture of concrete and rock. *Journal of Engineering Mechanics, ASCE* 1985; **111**(4):559–582.
12. Bažant ZP, Caner FC, Carol I, Adley MD, Akers SA. Microplane model M4 for concrete: I. Formulation with work-conjugate deviatoric stress. *Journal of Engineering Mechanics, ASCE* 2000; **126**(9):944–953.
13. Caner FC, Bažant ZP. Microplane model M7 for plain concrete I. Formulation, II. Calibration and verification. *Journal of Engineering Mechanics, ASCE* 2013; **139**:1714–1735.
14. Bažant ZP Microplane model for strain-controlled inelastic behavior. In Mechanics of Engineering Materials Chapter 3, Desai CS, Gallagher RH (eds). Wiley: London, 1984; 45–59.
15. Bažant ZP, Oh BH. Microplane model for fracture analysis of concrete structures. Proc., Symp. on the Interaction of Non-Nuclear Munitions with Structures, held at U.S. Air Force Academy, Colorado Springs, 1983; 49–53.
16. Bažant ZP, Kim JK. Creep of anisotropic clay: microplane model. *Journal of geotechnical engineering, ASCE* 1986; **112**(4):458–475.
17. Prat PC, Bažant ZP. Microplane model for triaxial deformation of saturated cohesive soils. *Journal of geotechnical engineering, ASCE* 1991; **117**(6):891–912.

DOI: 10.1002/nag

18. Bažant ZP, Zi G. Microplane constitutive model for porous isotropic rocks. *International Journal for Numerical and Analytical Methods in Geomechanics* 2003; **27**(1):25–47.
19. Yang Q, Chen X, Zhou WY. Microplane-damage-based effective stress and invariants. *International Journal of Damage Mechanics* 2005; **14**(2):179–191.
20. Murakami S. Mechanical modelling of material damage. *Journal of Engineering Materials and Technology: ASME* 1988; **55**(2):280–286.
21. Hill R. The Mathematical Theory of Plasticity. Clarendon Press: Oxford, 1950.
22. Liu C, Huang Y, Stout MG. On the asymmetric yield surface of plastically orthotropic materials: a phenomenological study. *Acta Materialia* 1997; **45**(6):2397–2406.
23. Oda M, Yamabe T, Ishizuka Y, Kumasaka H, Tada H. Elastic stress and strain in jointed rock masses by means of crack tensor analysis. *Rock Mechanics and Rock Engineering* 1993; **26**(2):89–112.
24. Swoboda G, Shen XP, Rosas L. Damage model for jointed rock mass and its application to tunnelling. *Computers and Geotechnics* 1998; **22**(3/4):183–203.
25. Kanatani K. Distribution of directional data and fabric tensors. *International Journal of Engineering Science* 1984; **22**(2):149–164.
26. Lubarda VA, Krajcinović D. Damage tensors and the crack density distribution. *International Journal of Solids and Structure* 1993; **30**(2):2859–2877.
27. Chen X, Yang Q, Qiu KB, Feng JL. An anisotropic strength criterion for jointed rock masses and its application in wellbore stability analyses. *International Journal for Numerical and Analytical Methods in Geomechanics* 2008; **32**(6):607–631.
28. Carol I, Bažant ZP. Damage and plasticity in microplane theory. *International Journal of Solids and Structure* 1997; **34**(29):3807–3835.
29. Gowd TN, Rummel F. Effect of confining pressure on the fracture behaviour of a porous rock. *International Journal of Rock Mechanics and Mining Science and Geomechanics Abstracts* 1980; **17**(4):225–229.
30. Jennings JE. A mathematical theory for the calculation of the stability of open cut mines. Proceeding of Symposium on the Theoretical Background to the Planning of Opening Pit Mines, Johannesburg, 1970; 87–102.
31. Carol I, Prat PC, Bažant ZP. New explicit microplane model for concrete: theoretical aspects and numerical implementation. *International Journal of Solids and Structure* 1992; **29**(9):1173–1191.

DOI: 10.1002/nag